Energy materials

Investigation of group 13 elements as potential candidates for *p*-type dopants in the narrow-gap thermoelectric semiconductor α-SrSi₂

Haruno Kunioka[1,*] , Daishi Shiojiri[1,2], Shinta Takahashi[1], Kota Hiratsuka[1], Masato Yamaguchi[1], Naomi Hirayama[3], Yoji Imai[1], Motoharu Imai[4], and Tsutomu Iida[1]

[1] *Department of Materials Science and Technology, Tokyo University of Science, Niijuku 6-3-1, Katsushika, Tokyo 125-8585, Japan*

[2] *Kanagawa Institute of Industrial Science and Technology, Electronics Engineering Department, Ebina-shi, Kanagawa, Japan*

[3] *Next Generation TATARA Co-Creation Centre, Shimane University, Matsue, Japan*

[4] *Research Center for Electronic and Optical Materials, National Institute for Materials Science, 1-2-1 Sengen, Tsukuba, Ibaraki 305-0047, Japan*

ABSTRACT

To investigate the possibility of *p*-type doping of α-SrSi₂, a promising as an eco-friendly thermoelectric material, the energy changes of substitutions of the Si site of α-SrSi₂ by group 13 elements were evaluated using first-principles calculations. It is found that Ga doping was the most energetically favorable dopant while In is the most unfavorable. We examined the synthesis of Ga- and In-doped α-SrSi₂ using the vertical Bridgeman method and investigated their thermoelectric properties. The Ga atoms were doped to α-SrSi₂ successfully up to 1.0 at. %, while In atoms could not be doped as suggested by calculations. For experimental prepared Ga-doped samples, the carrier density was observed to increase with Ga doping, from 3.58×10^{19} cm⁻³ for undoped α-SrSi₂ to 4.49×10^{20} cm⁻³ for a 1.0 at. % Ga-doped sample at 300 K. The temperature dependence of carrier concentrations was observed to change from negative to positive with increasing Ga content. In addition, the temperature dependence of the Seebeck coefficient was also observed to change from negative to positive with increasing Ga content. The results indicate that α-SrSi₂ undergoes a semiconductor–metal transition with Ga doping. The power factor for the undoped sample was quite high, at 2.5 mW/mK², while the sample with 0.3 at. % Ga had a value of 1.1 mW/mK² at room temperature.

Handling Editor: Kevin Jones.

Address correspondence to E-mail: kunioka@rs.tus.ac.jp

Introduction

One of the most promising means by which waste heat from industrial heating processes can be utilized to generate electricity is to use thermoelectric (TE) power generators employing TE conversion materials. Therefore, many kinds of thermoelectric material had been developed [1]. Bi-Te is a material that exhibits outstanding TE power generation performance around room temperature (RT), but due to the rarity of its constituent elements, alternative materials are being actively developed, such as (i) Mg-Ag-Sb [2–5], (ii) Fe-V-Al [6, 7], (iii) Zr-Ti-Ta/Ni–Sn [8–10], (iv) Mg_2SiSn [11, 12], (v) Al–Fe–Si [13, 14], and (vi) Cu_2Se [15]. The performance of these thermoelectric materials has been generally improved by doping. Not only but the doping concentration be also the carrier type can change. For example, various dopants were substituted into Mg_2Si and both p-type and n-type were realized [16–19]. From the viewpoint of the environmental impact, the sustainability of the materials used to construct it is of paramount importance and it is desirable for the materials to comprise elements that are non-toxic, resource abundant, easily recyclable, and inexpensive. Materials (i) through (iii) above have shown power generation capability comparable to Bi-Te, but cannot satisfy the sustainability requirements. Materials (iv) and (v) are environmentally benign materials, but would require improvements in their power density.

α-$SrSi_2$ is a sustainable narrow-gap semiconductor [20] and has demonstrated potential for power generation in the 100–300 °C range [21–23]. Undoped α-$SrSi_2$ has a promising power factor of 2.28 mW/mK^2 at 300 K [23]. We have focused on this material and have synthesized high-purity α-$SrSi_2$ by the vertical Bridgman method. The band gap was estimated from the temperature dependence of the carrier density, and the effects of isotropic strain and of the incorporation of isoelectronic impurities were determined from first-principles calculations [24, 25].

The substitution of Si atoms in α-$SrSi_2$ by group 13 elements is expected to enhance the TE properties because the dominant carrier of α-$SrSi_2$ is holes. However, the Bridgman method is a thermal equilibrium synthesis method which tends to be less prone to impurity substitution than previously reported non-equilibrium methods (e.g., arc-melt method) [24, 26–29]. Therefore, we focused on the formation energy, which is an index of the ease of substitution, and investigated the possibility of substituting

13 elements (B, Ga, In, and Al) to α-$SrSi_2$. In this paper, only the formation energy results are briefly discussed. The full details of these results including electronic structural calculations such as band structure and density of states will be reported separately, alongside results on the screening of dopants using group 15 elements [30].

Based on the results, α-$SrSi_2$ samples doped with the selected group 13 elements were prepared under thermal equilibrium conditions using a vertical Bridgman furnace, and the basic bulk matrix synthesis, impurity doping properties, basic electrical properties, and the TE properties were clarified. To evaluate the electrical and TE conversion properties, TE chips were formed by a plasma-activated sintering process.

Preliminary calculations for screening the dopant

Calculation method

First-principles calculations using density functional theory (DFT) were performed using the PW-SCF module of Quantum Espresso, a first-principles DFT calculation code that uses pseudopotentials [31]. Perdew–Burke–Ernzerhof (PBE) functionals were used to determine the total energy of the system based on the electron density distribution. These functionals are some of the most widely used in generalized gradient approximations (GGAs) [32]. For calculations of the doped and undoped systems, we performed structural relaxation calculations using the above PBE functionals. The calculations were performed for a $2 \times 2 \times 2$ supercell of the primitive unit cell of Sr_4Si_8. $Sr_{32}Si_{64}$ contains 64 Si atoms. Because all the Si atoms occupy the same crystallographic site, we chose one atom to substitute Si atom by a B, Al, Ga or In atom, which corresponds to substitution of 1.04 at. %.

The formation energy ΔE which shows the stability of the impurities in the α-$Sr_{32}Si_{64}$ was calculated by the following equation,

$$\Delta E\ (Sr_{32}Si_{63} : A) = E(Sr_{32}ASi_{63}) + E(Si) - E(Sr_{32}Si_{64}) - E(A) \quad (1)$$

where $E(Sr_{32}ASi_{63})$, $E(Sr_{32}Si_{64})$, $E(Si)$, and $E(A)$ are the total energies in each crystalline state.

Results of calculations for selecting the dopants

The lattice constants of α-$Sr_{32}Si_{63}A$ (A = Si, B, Al, Ga, In) determined by structural relaxation calculations and the formation energies calculated from Eq. 1 are plotted as functions of the sum of the covalent radii of Si and A in Fig. 1, with reference to Okada and Cordeo et al. Since the Si–Si bond length of 0.239 nm reported by J. Evers for undoped $SrSi_2$ is close to the covalent bond length [33], 0.2351 nm of the Si crystal with the diamond structure, each Si atom in $SrSi_2$ would have the same bonding nature with its neighboring Si atoms [34]. As shown in Fig. 1a, the lattice constant of α-$Sr_{32}Si_{63}A$ tends to increase as the sum of the covalent radii of Si and A increases, which indicates that there is no significant difference in the
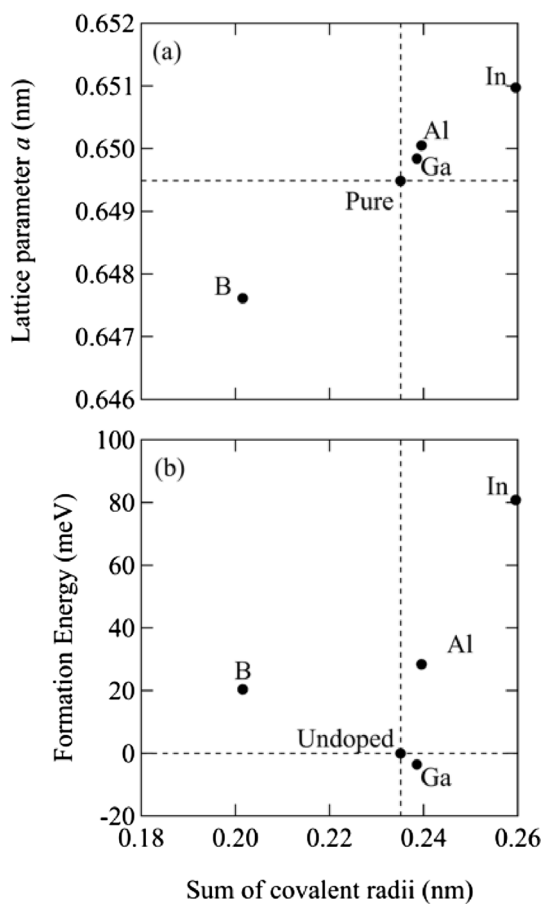
Figure 1 Sum of the covalent radii of Si and A (A = B, Ga, Al, In) dependence of **a** lattice parameter in α-$Sr_{32}Si_{63}$ A (A = B, Al, Ga, In), **b** formation energy of α-$Sr_{32}Si_{63}$ A (A = B, Al, Ga, In). The covalent radii are referenced from Okada et al. [34] on Si, and from Codero et al. for A [37].

bonding properties when a Si atom is replaced by a group 13 element.

It should be noted here that the lattice constant of undoped α-$Sr_{32}Si_{64}$ predicted by structural relaxation is 0.6495 nm, which is smaller than the experimentally reported minimum value of 0.6525 nm at 8.9 K [33]. This is due to the fact that the predicted lattice constant is for a temperature of 0 K, whereas the experimentally observed lattice constant is over 0 K. In addition, the reported experimental values also scatter from 0.6515 to 0.6535 nm (at about 300 K) due to different defect concentrations in the different fabrication methods [33, 35, 36]. These factors may cause small errors in the predicted lattice constant.

The formation energy, ΔE, of α-$Sr_{32}Si_{63}$ A from α-$Sr_{32}Si_{64}$ and A (approximately 1 at. % A) is plotted against the sum of the covalent radii of Si and A in Fig. 1b, which indicates how much the doped structure is stabilized by impurity doping. As shown in Fig. 1b, the formation energy of α-$Sr_{32}Si_{63}A$ tends to increase as the covalent bond length increases, except for when A = Ga. Therefore, among the group 13 elements, Ga seems to be the most stable when used to dope α-$SrSi_2$. The formation energy was as high as 80 meV for α-$Sr_{32}Si_{63}In$, where the difference between the sum of the covalent radii of Si and A and that of Si–Si is the greatest. More detailed information is given elsewhere [30]. From the preliminary calculations described above, except for Ga, the other group 13 elements are found to be energetically unfavorable as substitutes for Si in α-$SrSi_2$.

As targets for the actual experimental investigation, we have selected Ga as dopant for α-$SrSi_2$. In addition, to confirm whether elements with high formation energy is difficult to be substituted into α-$SrSi_2$, we have also selected In.

Experimental doping characteristics

Experimental methods

Samples were synthesized by the vertical Bridgeman method. The starting materials are 33.3: 66.7-*x: x* molar mixtures (0 < = x < = 1.0) of Sr (2.5N: Furuuchi Chemical Co., Ltd.), Si (5N: Kojundo Chemical Laboratory Co., Ltd.) and dopants (Ga (6N: Furuuchi Chemical) or In (5N: Furuuchi Chemical)). The starting material, weighed inside a globe box, was put into a boron nitride (BN)-coated alumina crucible and loaded

inside a vertical Bridgeman furnace. The details on the vertical Bridgeman furnace are described elsewhere [25]. The material was the heated in Ar atmosphere up to 1393 K, which is 10 K higher than the melting temperature of SrSi$_2$ [38]. After keeping the temperature at 1393 K for 3 h, the sample was moved downward at the speed of 36 mm/h. The resulting ingots were pulverized to powder with sizes of 25 ~75 μm in an Ar ambient and the samples for TE measurements then prepared by sintering the resulting powdered ingots. The powdered ingot put into a graphite die was sintered using a plasma-activated sintering apparatus (Elenix, Ed-PAS-III-Es). The sintering was performed at 1173 K for 10 min at a pressure of 100 MPa in an Ar (0.06 MPa) ambient to obtain a dense material. The true density of the resultants was measured using a Gas Displacement Pycnometry System (Micromeritics Instrument, AccuPycII 1340), and the relative density of the sintered pellet was estimated by the Archimedes method. The sintered samples were then cut using a wire saw.

The microstructure of the samples was examined using a scanning electron microscope (SEM; JEOL, JCM6000Plus). The distributions of the constituent elements, Sr and Si, and the incorporated dopants were observed by an energy-dispersive X-ray (EDX) spectrometer (JEOL, JED-2300). The grown crystals were characterized by powder X-ray diffractometry (XRD) with Cu Kα radiation (Rigaku, SmarLab). The compositions of grown specimens were determined by the XRD-Rietveld method. The standard material (Si, NIST 640e) was used in order to determine lattice constant from the powder XRD pattern. Hall coefficients were measured by the van der Pauw method under a magnetic field of 0.5 T at temperatures ranging from 80 to 400 K (Toyo, ResiTest 8300). The TE properties, including the Seebeck coefficient and the electrical conductivity, were measured over the temperature range from RT to 573 K using a Seebeck Coefficient/Electric Resistance Measurement System (Advance-Riko, ZEM-3), from which the power factor was estimated. The Seebeck coefficient was evaluated from plots of the ΔT-ΔV curves (where ΔT ≈ 5 K).

Results of the synthesis of Ga- and In-doped α-SrSi$_2$ and their electric and thermoelectric properties

We synthesized samples from 33.3: 66.7-x: x molar mixtures of Sr, Si, and dopants (Ga or In) using the vertical Bridgeman method. In the following, Ga$_x$ or In$_x$ is used to refer to the sample prepared from 33.3: 66.7-x: x molar mixtures of Sr, Si, and Ga or In. A photograph of the Ga0.3 sample is shown in Fig. 2a. The grown crystal has a maximum radius of 21 mm and a height of about 20 mm and did not adhere to the BN-coated Al$_2$O$_3$ crucible. The general appearance of this sample is similar to that of all the other doped and undoped samples. Figure 2b–f shows the back-scattered electron (BSE) images observed by SEM in the lower part of samples. Local elemental contents were measured at the points indicated by the numbers 1 to 11 in Fig. 2b–f. The results are summarized in Table 1. In all the samples, the matrix consists of SrSi$_2$, although the observed ratio of Si content to Sr content is slightly greater than the ideal ratio of Si content.

In the Ga-doped samples, the observed Ga content in the SrSi$_2$ matrix is close to the Ga content in the starting materials, suggesting that Ga atoms were doped into SrSi$_2$ successfully. The black area at position 2 in Fig. 2b is Si at the grain boundary, which we consider to be unreacted. These black areas are also observed in Fig. 2c and d, and it appears that the existence of Si at the grain boundary occurs regardless of the amount of Ga doping. For the upper part of each doped sample, i.e., that cut from between the center and the upper part, mainly Sr and Si elements were detected, but Si precipitation was observed as in the lower part. If the growth rate is sufficiently slow, Si in the Sr–Si eutectic microstructure should be excluded to the top, but the observation of Si regardless of the crystal location suggests that the growth rate is too fast.

As the amount of Ga added increases from 0.3 at. % to 1.0 at. %, a linear increase in the amount of Ga measured by SEM–EDX elemental analysis is observed. However, the composition becomes Si-rich as the Ga content increases. The BSE images of Ga1.0 (Fig. 2d) shows a surface morphology that is quite different from those with Ga0.3 and Ga0.5. While Ga and Si precipitation appears to be significantly reduced in this sample, grains and voids different from those observed in other samples of α-SrSi$_2$ seem to have formed. This indicates the need to investigate the solid solubility limit of Ga based on structural and other analyses. As the composition of the samples prepared in this study was only measured by EDX, it would be necessary to investigate the composition in detail by EPMA in the future to determine the exact concentration of the substituted impurities.

Figure 2 **a** Photograph of the cross section of the Ga0.3 sample and BSE images of **b** Ga0.3, **c** Ga0.5, **d** Ga1.0, **e** In0.5, and **f** Ga1.0. The numbers in the images indicate the positions where chemical compositions were analyzed by EDX.
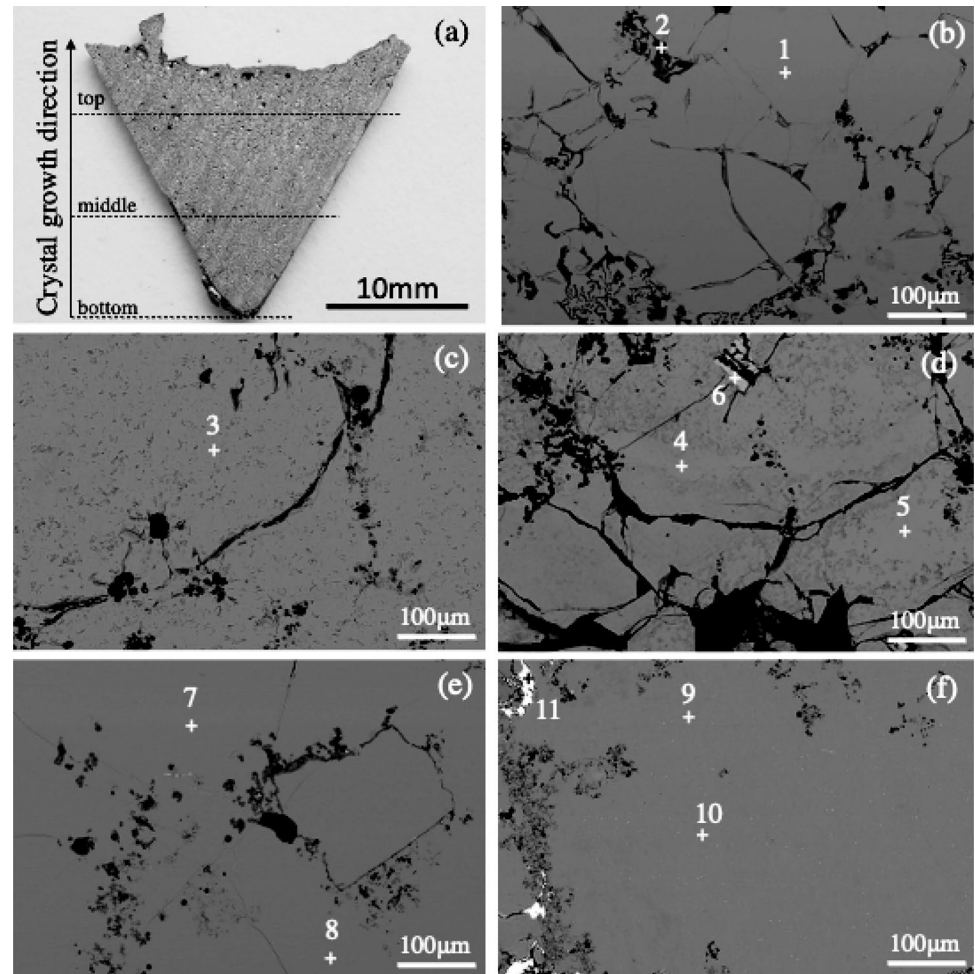
Table 1 Dopants, dopant contents in the starting materials, position, observed contents, and observed phases of undoped and doped $SrSi_2$

Sample	Impurity	Impurity content in the starting material (at. %)	Point number	Observed contents (at. %)			Observed phase
				Sr	Si	Impurity	
Undoped	-	-	-	32.6	67.4	-	$SrSi_2$
Ga0.3	Ga	0.3	1	32.7	66.9	0.34	$SrSi_2$
			2	0.00	100	0.00	Si
Ga0.5	Ga	0.5	3	32.3	67.2	0.47	$SrSi_2$
Ga1.0	Ga	1.0	4	30.9	68.0	1.18	$SrSi_2$
			5	31.0	68.1	0.95	$SrSi_2$
			6	32.6	44.8	22.6	$SrGa_xSi_{2-x}$
In0.5	In	0.5	7	32.8	67.2	0.031	$SrSi_2$
			8	32.8	67.2	0.00	$SrSi_2$
In1.0	In	1.0	9	28.7	71.2	0.051	$SrSi_2$
			10	28.7	71.3	0.012	$SrSi_2$
			11	1.2	1.8	97.0	In

In Ga1.0 (Fig. 2d), a light gray precipitate was observed at the position 11. The ratio of Sr, Si, and Ga in this region is approximately 3:4:2, which suggests that this precipitate is a ternary compound $SrGa_xSi_{2-x}$ with the AlB_2-type structure [39–42]. The solid solubility limit of Ga in $SrSi_2$ is deduced to be approximately 1.0 at. %, because the Ga content in $SrSi_2$ is approximately 1.0 at. % and $SrGa_xSi_{2-x}$ appears in Ga1.0, but not in Ga0.5.

In contrast to the Ga-doped samples, the In-doped samples shown in Fig. 2e and Fig. 2f (0.5 at. % and 1.0 at. %, respectively) show observed In contents in the $SrSi_2$ grain much smaller than those in the starting materials. On the other hand, as shown in Fig. 2e, metallic In crystallized near the α-$SrSi_2$ grain boundaries. In the In-doped sample, residual Si, and metallic In were present as eutectic ejecta at the top of the sample. Compared to the change in lattice parameter and formation energy when In is introduced, which were calculated by the first-principles calculations performed as screening in this study, these experimental data indicate that it is difficult to introduce In in a substitutional form in an actual thermodynamically stable environment.

Figure 3 shows the results of powder XRD analysis for α-$SrSi_2$ samples grown by the vertical Bridgman method from source materials containing 1.0, 0.5 at. % In and 1.0, 0.5, and 0.3 at. % Ga, respectively. These XRD measurements reveal that the composition of the material obtained in this study is mainly α-$SrSi_2$ (cubic, space group: $P4_132$), which exhibits a semiconducting phase. In the XRD spectra, a metallic phase β-$SrSi_2$ (tetragonal, space group: $I4_1/amd$) was not observed in the undoped, Ga-doped, and In-doped samples, whereas α-$SrSi_2$ and a slight peak indicating residual Si, possibly due to the evaporation of Sr, were observed.

Ga is not observed in the XRD spectra, whereas clear peaks indicating In precipitates can be observed, in agreement with the SEM observations. The value of the peak increases with the concentration of the impurity.

Since lattice parameter changes are expected to vary with the amount of impurity elements substituted, the lattice parameter values with observed impurity content are listed in Table 2, along with the content of Ga or In in the grains as determined by EDX. The

Table 2 Observed impurity content and lattice constant of undoped and doped α-$SrSi_2$. The number of the parenthesis at lattice constant represents the standard deviation

| Sample	Observed Impurity content (at. %)	Lattice constant (nm)
Undoped	–	0.6535(1)
Ga0.3	0.34	0.6536(1)
Ga0.5	0.47	0.6537(1)
Ga1.0	1.18	0.6538(1)
In0.5	0.03	0.6535(1)
In1.0	0.05	0.6535(1)

Figure 3 RT X-ray diffraction patterns of α-$SrSi_2$ samples grown by the vertical Bridgman method from source materials containing 1.0, 0.5 at. % In (In1.0, In0.5) and 1.0, 0.5, and 0.3 at. % Ga (Ga0.3, Ga0.5, Ga1.0), or without (undoped), respectively.
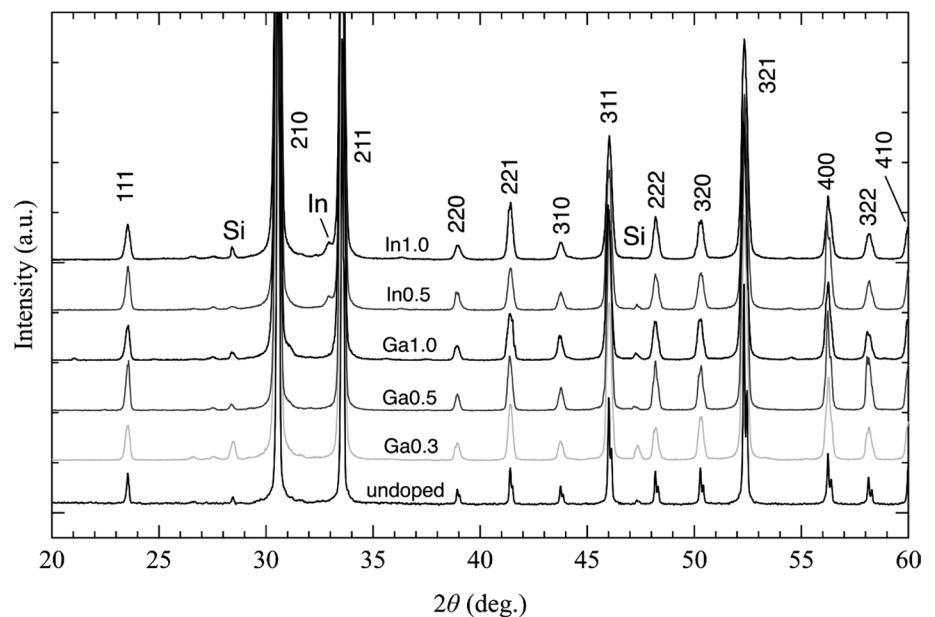
lattice constant of undoped α-SrSi$_2$ is 0.6535(1) nm, which is consistent with previously reported values [33, 35, 36]. The lattice constant of the Ga-doped sample increases with increasing Ga content in the grains. On the other hand, the In-containing samples have almost no In content in the grains and therefore show no increase in the lattice constant. This suggests that the lack of change in the lattice constant is due to the lack of In substitution within α-SrSi$_2$. The observation is consistent with the calculation result which showed a high formation energy and a likely instability for the substitution of In on a Si site. However, the impurity content determined by EDX shows information within the grain only at one localized location. On the other hand, when evaluating thermoelectric properties, we are looking at the properties not only within the grains, but also at the grain boundaries and precipitates. Therefore, this impurity content trend within the grains does not always match the properties.

The lattice parameters calculated from XRD measurements for α-SrSi$_2$ samples grown by the vertical Bridgman method from source materials containing 1.0, 0.5 at. % In and 1.0, 0.5, and 0.3 at. % Ga, respectively, are plotted as functions of the source materials in Fig. 4. For the Ga-doped sample, the lattice constant value tends to increase with Ga doping. When Ga is doped 1 at. %, the lattice constant is increased by 0.04% compared to the undoped lattice constant. Comparing this rate of increment with the calculated results, the calculated lattice parameter is increased by 0.05% by doping Ga into α-SrSi$_2$, which is the same
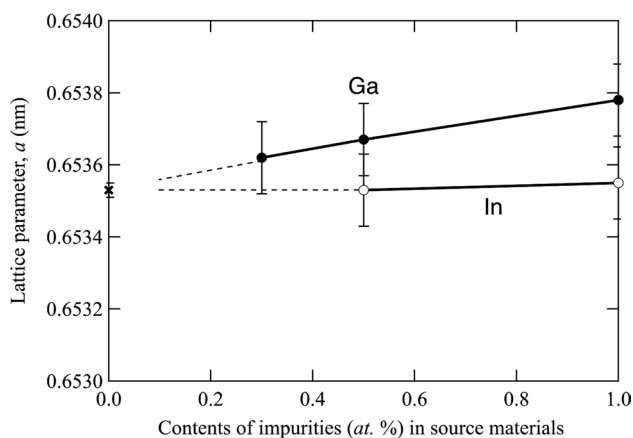
Figure 4 Lattice parameter at RT of α-SrSi$_2$ samples grown by the vertical Bridgman method from source materials containing 1.0, 0.5 at. % In and 1.0, 0.5, and 0.3 at. % Ga, or without, respectively.

rate of increment as in the experimental results. Since the experimental results are in accordance with the first-principles calculations, it is considered to be substituted at the Si site and behave as a p-type dopant. The sample with 1.0 at. % Ga showed a different surface morphology from the 0.3 at. % and 0.5 at. % samples as seen in the SEM observations.

The change in lattice parameter shown in Fig. 4 may be taken as an indication of the changes seen in the 0.3 at. % and 0.5 at. % samples. If Ga is a p-type impurity, the next thing to determine is the status of the electrical activation after substitution at the Si sites. This was done by electrical measurements and these are discussed in the next section. The electrical activation of the sample with 1.0 at. % Ga is particularly interesting because this is not a small amount of impurity. On the other hand, for the In-doped samples, no noticeable change in the lattice constant of the undoped α-SrSi$_2$ was observed with increasing amounts of In. Considering this result, it is reasonable to assume that the experimental process conditions used here to add In to α-SrSi$_2$ are unsuitable for the substitution of In at Si sites.

Unfortunately, the samples grown in this experiment had many voids and weak grain boundaries, as shown in Fig. 2, and were not structurally or thermally stable, so it was not possible to directly cut sample pieces from the grown samples to measure the electrical and thermoelectric properties. Therefore, to measure the electrical and thermoelectric properties, a process was introduced to prepare specimen pieces by grinding and sintering (plasma-activated sintering) the grown samples. Referring to the experimental data which shows that the In-doped samples did not form a solid solution with α-SrSi$_2$, we decided only to measure the electrical and thermoelectric properties of the Ga-doped samples. Hereafter, we simply express the sample obtained from the source material containing, for example, 0.5 at. % Ga as "0.5 at. % Ga-doped."

Figure 5 shows BSE images of observations of the surfaces of the undoped and Ga-doped samples sintered by the plasma-activated sintering method. The relative densities of all the samples were over 95~96%. Crack and void-free samples were obtained, and the sintering produced sufficiently dense samples to enable measurements of the electrical and thermoelectric properties. No significant difference in morphology was observed between the Ga-doped and undoped samples. Local elemental analysis revealed that the crystal grains were mainly formed of SrSi$_2$. In all

Figure 5 SEM image (back-scattered electron image) of **a** undoped α-SrSi$_2$, and α-SrSi$_2$ doped with **b** 0.3 at. % Ga, **c** 0.5 at. % Ga and **d** 1.0 at. % Ga sintered by a plasma-activated sintering technique.
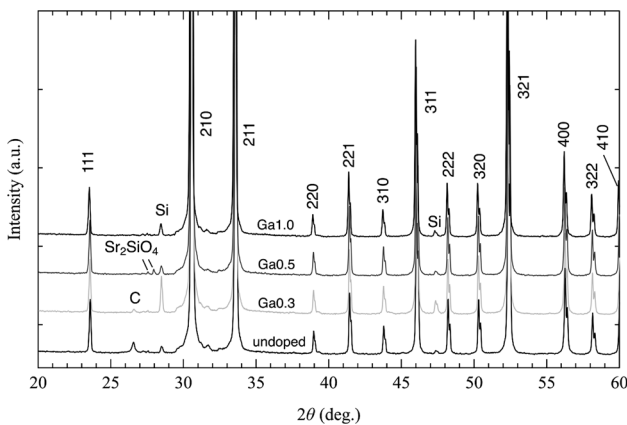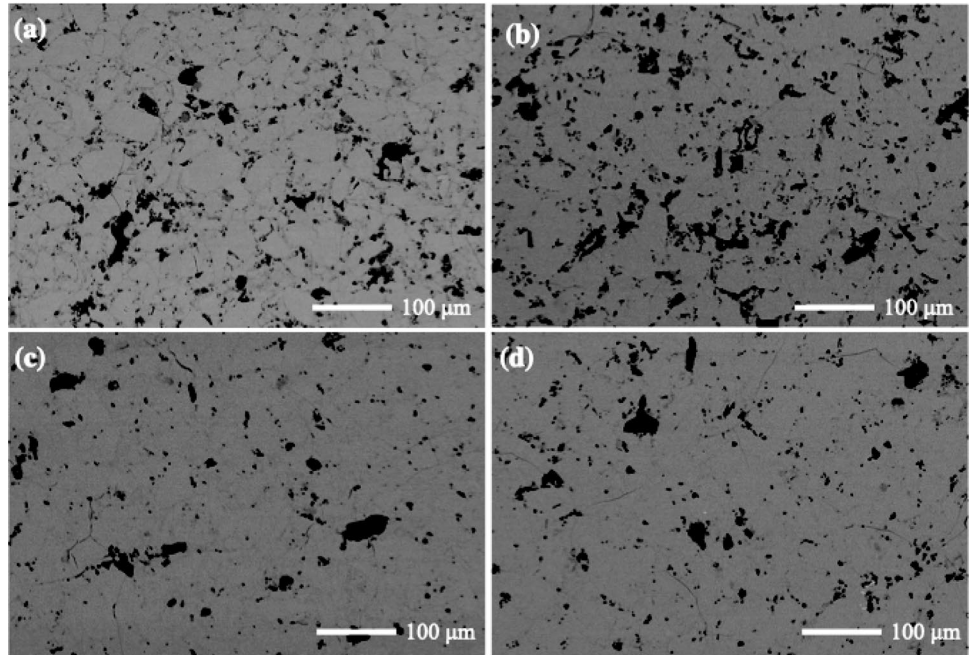
Figure 6 X-ray diffraction patterns of undoped α-SrSi$_2$, and α-SrSi$_2$ doped with 0.3 at. % Ga (Ga0.3), 0.5 at. % Ga (Ga0.5) and at. % 1.0 Ga (Ga1.0) sintered by a plasma-activated sintering technique.

samples, Si, which is observed in vertical Bridgeman samples, is also observed in PAS samples. In addition, precipitates with a high content of SrGa$_x$Si$_{2-x}$, which were observed in Ga1.0, were also present at the grain boundaries.

Figure 6 shows powder XRD patterns of the sintered undoped and Ga-doped samples. These XRD patterns indicate that the sintered samples mainly consist of α-SrSi$_2$. Small amounts of impurities were observed. In all the sintered samples, a trace of diffraction peaks

from Si was observed at 28.4 degree. Additional small diffraction peaks were observed in the sintered samples. The small diffraction peaks from Sr$_2$SiO$_4$ were observed in Ga0.5 and an unidentified small peak, indicated by C, was observed at 26.6 degree in Ga0.3. We believe that the effect of these impurities on transport and TE properties is small because the amount of these impurity is deduced to be small from the small diffraction peak intensity from the impurities compared with those from α-SrSi$_2$.

Figure 7a shows an Arrhenius plot of the carrier density of sintered undoped and Ga-doped samples in the temperature range from 80 to 400 K. For the undoped sample, the temperature dependence of n can be expressed by the equation that describe a typical temperature dependence of intrinsic carrier density for semiconducting materials:

$$n = AT^{\frac{3}{2}} exp\left(-\frac{E_g}{2k_BT}\right) \qquad (2)$$

where A, k$_B$, and E$_g$ are constant, the Boltzmann constant, and band gap, respectively. A band gap of 49.2 meV is obtained by fitting of the data at temperatures from 270 to 400 K to Eq. 2.

Our previous SrSi$_2$ samples, which were predominantly α-SrSi$_2$ with a small amount of β-SrSi$_2$ and residual Si, had a bandgap of about 13 meV over approximately the same temperature range [25]. In

Figure 7 Results of the electrical measurements for undoped and Ga-doped α-SrSi$_2$ specimens: **a** carrier density, **b** Hall mobility.
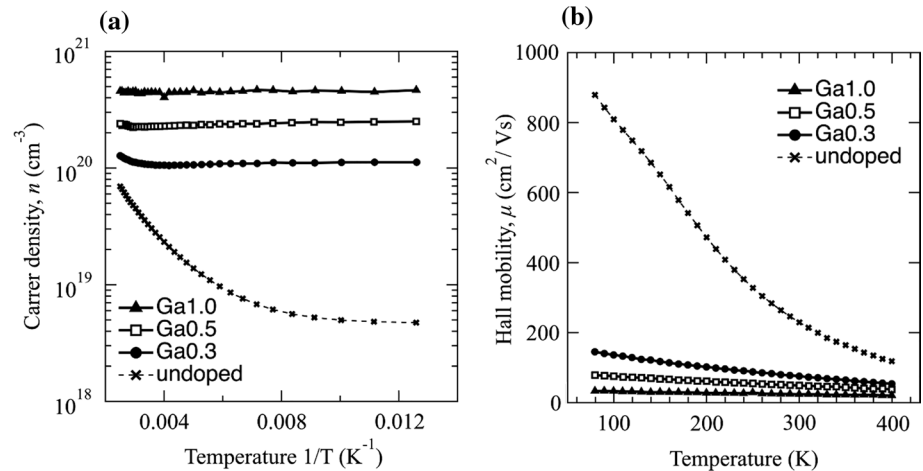
addition, the carrier density in the low-temperature range of the samples prepared in this study was lower than that of the samples prepared in the previous study. At present, improving the process for preparing α-SrSi$_2$ single-phase crystals is in a state of exploration, but we consider that the process used in this study has improved the quality of the undoped samples compared to the process we used in the past. These results suggest that we successfully improved the quality of samples in the present study. The bandgap of undoped α-SrSi$_2$ is reported to be about 34 meV for a sample prepared by a combination of melt synthesis using an arc-melt method and subsequent plasma-activated sintering [20], so it depends somewhat on the preparation process. The bandgap of α-SrSi$_2$ has been shown to be very narrow, based on first-principles calculations [28] and experiments, so it may be difficult to evaluate it as an absolute physical property.

In the samples with Ga as a *p*-type impurity, it seems that the carrier density increases proportionally with increasing amounts of Ga content. For example, the carrier concentrations at 400 K were 7.1×10^{19} cm^{-3} for undoped sample, 1.3×10^{20} cm^{-3} for Ga0.3, 2.4×10^{20} for Ga0.5, and 4.6×10^{20} for Ga1.0. Based on the octet rule and considering the valence, the valence of Sr, Si, and Ga are $2+$, $4+$, and $3+$, respectively. Since the carrier density increased proportionally with increasing Ga doping, the added Ga is considered to be substituted into the Si site. The Ga content of the sample after sintering determined by EDX is 0.23 at. % for Ga0.3, 0.53 at. % for Ga0.5, and 1.0 at. % for Ga1.0. Thus, carrier density seems to increase with Ga content linearly. Although it is necessary

to conduct secondary ion mass spectrometry (SIMS) measurements to evaluate the exact values of the electrical activation rates for the amount of Ga added, it is seen that electrical activation with the added Ga is somewhat high. As the concentration of incorporated Ga increases, it becomes difficult to find a clear activation energy from the temperature dependence of the carrier concentration, but a bandgap of 16 meV can be calculated for the sample with 0.3 at. % Ga in the temperature range from 80 to 400 K. The determination of band gap becomes difficult in the sample with higher Ga content. In Ga1.0, the carrier density is almost independent of temperature, suggesting that at Ga1.0 it is like a metal. This phenomenon is not limited to the case of Ga doping, since α-SrSi$_2$ also behaves with metallic character when α-SrSi$_2$ is doped with aluminum, which acts as a p-type dopant [28].

Such a phenomenon commonly can be caused by the Fermi level, which is located in the middle of the band gap, being lowered by doping and touching the valence band, or by a change in the band structure, resulting from a collapsed band gap.

The band structure of α-Sr$_{32}$Si$_{63}$Ga doped with 1 at. % Ga reported by D. Shiojiri et al. revealed that the band gap is in fact collapsed, and that the position of the Fermi level shifts toward the valence band [30]. The sample in this study is assumed to have exhibited metallic behavior due to the change in band structure and the lowering of the Fermi level by doping Ga.

Figure 7b shows the Hall mobility μ of sintered undoped and Ga-doped α-SrSi$_2$ in the temperature range from 80 to 400 K. Hall mobility was obtained using the relation: $\sigma = ne\mu$, where e and σ are elemental charge and electrical conductivity, respectively. In

contrast to the undoped sample, a large decrease in the Hall mobility is observed in the Ga-doped samples, and the decrease is greater as the amount of Ga added increases. It should be noted that the undoped sample was not an as-grown single crystal sample, but a sintered powder sample. The sample measured is a sintered body with crystal grains of several tens of micrometers in size with many grain boundaries. Therefore, it is thought that the presence of crystal grains has a significant influence on the mobility measurement. Or we speculate that the Si network in α-SrSi$_2$, which can be playing a role in the electronic conduction, has become disordered by substituting Ga into the Si site of α-SrSi$_2$ which causes the mobility to decrease rapidly with increased Ga doping.

Figure 8 shows the measured temperature dependence of the electrical conductivity (Fig. 8a) and the Seebeck coefficient (Fig. 8b) for sintered undoped and Ga-doped α-SrSi$_2$. The temperature range measured was from RT to 573 K, this being the temperature range for low-temperature waste heat. The power factor (PF) shown in Fig. 8c is a reference value to determine the power generation capability of this material when used as a thermoelectric generator, and was calculated by PF = S$^2\sigma$, where S and σ are the Seebeck coefficient and electrical conductivity, respectively.

The positive value for the Seebeck coefficient for all the samples over the measured temperature range indicates that predominant charge carriers are holes. The sample showed a positive value without doping and this tendency is common within previous reports [21–23, 27].

The results of a formation energy calculation of a defected sample reported by D. Shiojiri indicate that Si defects are energetically more stable than Sr defect samples [43]. In view of the reported results, it is possible that the undoped sample shows p-type conduction due to a Si deficiency.

The Seebeck coefficient observed in the undoped sample has a maximum value of 135 μV/K at RT and then monotonically decreases with increasing temperature. In silicide TE materials, it is common to enhance the PF by adding impurities to increase the number of carriers, but at the present sample, when the impurity Ga is added to α-SrSi$_2$, the Seebeck coefficient is observed to decrease to a much lower value as seen in metallic TE materials. The Ga-doped α-SrSi$_2$ samples show slight monotonic increases with increasing temperature, although the 0.3 at. % Ga-doped sample has a rather flat characteristic over the measured
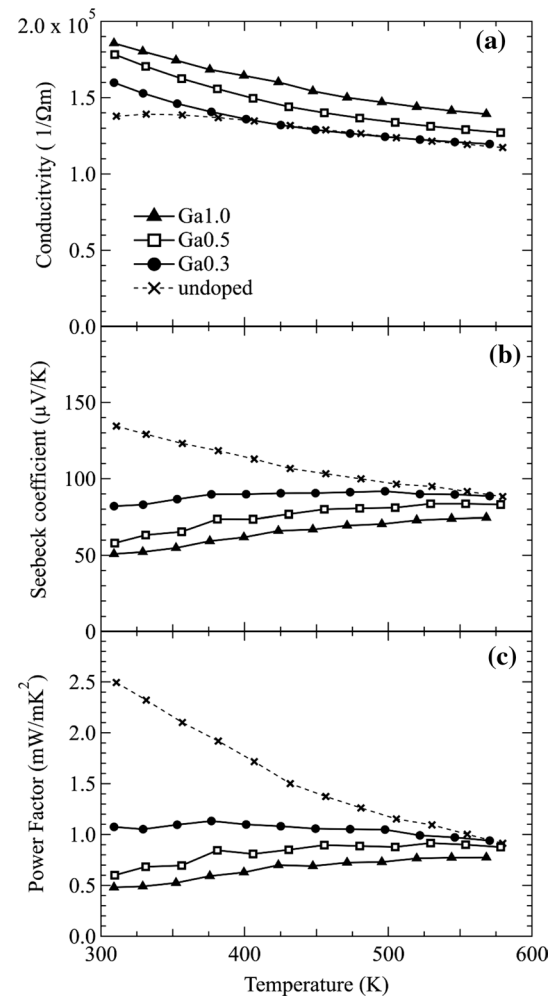
Figure 8 Thermoelectric properties of undoped and Ga-doped specimens as a function of the sample temperature ranging from RT to 573 K. **a** Electrical conductivity, **b** Seebeck coefficient, and **c** calculated power factor.

temperature range. S of Ga-doped samples decreases with increasing Ga content.

The electrical conduction characteristics shown in Fig. 8b can be viewed as characteristic values that are basically inversely correlated with the Seebeck coefficient characteristics, and the results obtained are in accordance with the Seebeck coefficient characteristics. The samples with 0.5 at. % and 1.0 at. % Ga concentration exhibit metallic behavior as far as the temperature dependence of electrical conductivity is concerned. This seems to be related to the fact that for these two Ga-doped concentrations, it was not possible to calculate the bandgap from the plots of the temperature dependence of the carrier concentration. On the other hand, the observed electrical conductivity

of the undoped sample and the sample with 0.3 at. % Ga is comparable over a wide temperature range, again showing a trend toward metallic behavior with increasing temperature. In addition, since the amount of incorporated impurities is on the order of 10^{20} cm^{-3}, it is possible that localized levels are formed at the band edge due to the introduction of defects associated with the incorporation of the impurities. In addition, the sample used for thermoelectric characterization is a sintered sample made from raw powder materials, which may be a factor that disturbs the band-edge portion of the sample crystal. The process-dependent and highly doped crystalline state of the sample and the narrow-bandgap properties of α-SrSi$_2$ may be of significance in understanding the thermoelectric property results. In order to confirm these initial findings, our first priority is to prepare a single crystal of α-SrSi$_2$ and obtain electrical and thermoelectric properties similar to those of the present experiment using a crystal sample in the as-grown condition.

The undoped sample has a rather high value of 2.5 mW/mK^2 at RT as shown in Fig. 8c. Considering just the PF values, the values obtained reach a level that allows the design of thermoelectric devices that can be expected to generate enough electricity for practical use. It is notable that this high value is shown for the undoped state without impurities added. Since undoped samples may contain unexpected impurities due to process contaminants or the level of purity of the raw material, it is necessary to investigate the residual impurities in more detail and their thermoelectric behavior in α-SrSi$_2$. The power factor at RT decreases with increasing Ga content, suggesting that the decrease in S is more dominant than the increase in σ for the change in PF. The value of it is 1.1 mW/mK^2 in the sample with 0.3 at. % and 0.5 mW/mK^2 in the sample with 1.0 at. %.

Conclusions

Impurity elements to be doped into α-SrSi$_2$ were selected based on the formation energy of group 13 substitutions into the Si site of α-SrSi$_2$ determined from first-principles calculations by density functional theory (DFT) with the Perdew–Burke–Ernzerhof functional.

We selected Ga and In for impurity elements, and samples were then prepared by the vertical Bridgeman method. The grown samples consisted mainly of α-SrSi$_2$, the semiconducting phase, with only a small amount of residual Si. For the impurity Ga, a tendency toward a solid solution and electrical activation of the α-SrSi$_2$ with an increase in lattice constant were observed for concentrations ranging from 0.3 at. % to 1.0 at. %. On the other hand, with the vertical Bridgeman method used in this study, the incorporation of In showed almost no solid solution in the range from 0.5 at. % to 1.0 at. %. Although the melt-synthesized samples were almost single-phase material, there were voids and cracks in the as-grown state, so the samples were subjected to a plasma-activated sintering process to prepare them for evaluation of their electrical properties. The temperature dependence of the carrier density in samples with densities above 97% resulted in activation energies corresponding to bandgaps of 49 meV for the undoped sample and 16 meV for the 0.3 at. % Ga-doped sample. The Seebeck coefficient and electrical conductivity of undoped and Ga-doped α-SrSi$_2$ were investigated. The undoped sample had a substantially higher value of 2.5 mW/mK^2 at RT compared to the sample with 0.3 at. % Ga, which had a value of 1.1 mW/mK^2 at RT.

Author contributions

Haruno Kunioka was involved in conceptualization, investigation, formal analysis, and writing—original draft. Daishi Shiojiri was responsible for conceptualization, investigation, and formal analysis. Shinta Takahashi, Kota Hiratsuka, and Masato Yamaguchi carried out investigation and formal analysis. Naomi Hirayama assisted with reviewing and editing. Yoji Imai helped with writing—reviewing and editing. Motoharu Imai contributed to conceptualization, funding acquisitions, and reviewing and editing. Tsutomu Iida took part in conceptualization, supervision, and writing—reviewing and editing.

Funding

Data and code availability

Data will be made available on request. All data included in this study are available upon request by contact with the corresponding author.

Declarations

Conflict of interest No potential conflict of interest was reported by the authors.

Ethical approval This manuscript does not involve human tissue or related experiments.

References

[1] Materials R-P (2016) G. Tan, L.-D.Z., Kanatzidis, M.G. Chem Rev 116:12123–12149. https://doi.org/10.1021/acs.chemrev.6b00255

[2] Liu Z, Wang Y, Mao J, Geng H, Shuai J, Wang Y, He R, Cai W, Sui J, Ren Z (2016) Lithium doping to enhance thermoelectric performance of MgAgSb with Weak Electron-Phonon Coupling. Adv Energy Mater 6:1502269. https://doi.org/10.1002/aenm.201502269

[3] Liu Z, Zhang Y, Mao J, Gao W, Wang Y, Shuai J, Cai W, Sui J, Ren Z (2017) The microscopic origin of low thermal conductivity for enhanced thermoelectric performance of Yb doped MgAgSb. Acta Materialia 128, 227–234. https://doi.org/10.1016/j.actamat.2017.02.015

[4] Wieder A, Camut J, Duparchy A, Deshpande R, Cowley A, Müller E, de Boor J (2023) High-performance tellurium-free thermoelectric module for moderate temperatures using α-MgAgSb/Mg$_2$(Si,Sn). Mater Today Energy 38, 101420. https://doi.org/10.1016/j.mtener.2023.101420

[5] Huang Y, Lei J, Chen H, Zhou Z, Dong H, Yang S, Gao H, Wei T-R, Zhao K, Shi X (2023) Intrinsically high thermoelectric performance in near-roomtemperature α-MgAgSb materials. Acta Mater 249:118847. https://doi.org/10.1016/j.actamat.2023.118847

[6] Lue CS, Kuo Y-K (2002) Thermoelectric properties of the semimetallic Heusler compounds Fe$_{2-x}$V$_{1+x}$M (M = Al, Ga). Phys Rev B 66:085121. https://doi.org/10.1103/PhysRevB.66.085121

[7] Fukuta K, Tsuchiya K, Miyazaki H, Nishino Y (2022) Improving thermoelectric performance of Fe$_2$VAl-based Heusler compounds via high-pressure torsion. Appl Phys A 128:184. https://doi.org/10.1007/s00339-022-05329-y

[8] Douglas JE, Birkel CS, Verma N, Miller VM, Miao M-S, Stucky GD, Pollock TM, Seshadri R (2014) Phase stability and property evolution of biphasic Ti–Ni–Sn alloys for use in thermoelectric applications. J Appl Phys 115:043720. https://doi.org/10.1063/1.4862955

[9] Gong B, Liu F, Zhu J, Wang X, Ao W, Zhang C, Li Y, Li J, Xie H (2019) Effects of Sc, Ti, Hf, V, Nb and Ta doping on the properties of ZrNiSn alloys. J Mater Sci 54:10325–10334. https://doi.org/10.1007/s10853-019-03623-4

[10] Yang X, Wang Y, Min R, Chen Z, Guo E, Kang H, Li L, Jiang X, Wang T (2022) Enhancement in thermoelectric properties of ZrNiSn-based alloys by Ta doping and Hf substitution. Acta Mater 233:117976. https://doi.org/10.1016/j.actamat.2022.117976

[11] Liu W, Tan X, Yin K, Liu H, Tang X, Shi J, Zhang Q, Uher C (2012) Convergence of conduction bands as a means of enhancing thermoelectric performance of n-Type Mg$_2$Si$_{1-x}$Sn$_x$ solid solutions. Phys Rev Lett 108:166601. https://doi.org/10.1103/PhysRevLett.108.166601

[12] Cheng K, Bu Z, Tang J, Zhang X, Meng X, Li W, Pei Y (2022) Efficient Mg$_2$Si$_{0.3}$Sn$_{0.7}$ thermoelectrics demonstrated for recovering heat of about 600 K. Mater. Today Phys. 28, 100887. https://doi.org/10.1016/j.mtphys.2022.100887

[13] Hou Z et al (2021) First–principles study of electronic structures and elasticity of $Al_2Fe_3Si_3$. J Phys: Condens Matter 33, 195501. https://doi.org/10.1088/1361-648X/abe474

[14] Takagiwa Y, Isoda Y, Goto M, Shinohara Y (2018) Conduction type control and power factor enhancement of the thermoelectric material $Al_2Fe_3Si_3$. J Phys Chem Solids 118:95–98. https://doi.org/10.1016/j.jpcs.2018.03.003

[15] Butt S, Farooq MU, Mahmood W, Salam S, Sultan M, Basit MA, Ma J, Lin Y, Nan C-W (2019) One-step rapid synthesis of Cu_2Se with enhanced thermoelectric properties. J Alloys compd 786:557–564. https://doi.org/10.1016/j.jallcom.2019.01.359

[16] You S-W, Park K-H, Kim I-H, Choi S-M, Seo W-S, Kim S-U (2012) Solid-State synthesis and thermoelectric properties of Al-Doped Mg_2Si. J Electron Mater 41:1675–1679. https://doi.org/10.1007/s11664-011-1786-7

[17] Muthiah S, Sivaiah B, Gahtori B, Tyagi K, Srivastava AK, Pathak BD, Dhar A, Budhani RC (2014) Double-Doping approach to enhancing the Thermoelectric Figure-of-Merit of n-Type Mg_2Si synthesized by use of spark plasma sintering. J Electron Mater 43:2035–2039. https://doi.org/10.1007/s11664-013-2944-x

[18] Tada S, Isoda Y, Udono H, Fujiu H, Kumagai S, Shinohara Y (2014) Thermo-electric properties of p-Type $Mg_2Si_{0.25}Sn_{0.75}$ doped with sodium acetate and metallic sodium. J Electron Mater. 43, 1580–1584. https://doi.org/10.1007/s11664-013-2797-3

[19] Meng QS, Fan WH, Chen RX, Munir ZA (2011) Thermoelectric properties of Sc-and Y-doped Mg_2Si prepared by field-activated and pressure-assisted reactive sintering. J Alloys compd 509:7922–7926. https://doi.org/10.1016/j.jallcom.2011.05.033

[20] Imai M, Naka T, Furubayashi T, Abe H (2005) Electrical properties of polycrystalline $SrSi_2$. Appl Phys Lett 86:032102. https://doi.org/10.1063/1.1849423

[21] Hashimoto K, Kurosaki K, Imamura Y, Muta H, Yamanaka S (2007) Thermoelectric properties of $BaSi_2$, $SrSi_2$. J Appl Phys 102:5063703. https://doi.org/10.1063/1.2778747

[22] Kuo YK, Ramachandran CSLB (2014) Optimization of thermoelectric performance of $SrSi_2$-based alloys via the modification in band structure and phonon-point-defect scattering. Front Chem 2:2296–2646. https://doi.org/10.3389/fchem.2014.00106

[23] Singh SK, Imai M (2020) Thermoelectric properties of cubic Ba-substituted strontium disilicide, $Sr_{1-x}Ba_xSi_2$, with Ba content above solid solubility limit. Inter- metallics 127:106981. https://doi.org/10.1016/j.intermet.2020.106981

[24] Shiojiri D, Iida T, Yamaguchi M, Hirayama N, Imai1 Y (2021) Electronic structure tuning of α-$SrSi_2$ by isotropic strain and isoelectronic impurity incorporation: A first-principles study for enhancement of low-temperature thermoelectric performance. J Appl Phys 130, 215103. https://doi.org/10.1063/5.0063506

[25] Shiojiri D, Iida T, Kadono T, Yamaguchi M, Kodama T, Yamaguchi S, Takahashi S, Kayama Y, Hiratsuka K, Imai M, Hirayama N, Imai Y (2021) Re-evaluation of the electronic structure and thermoelectric properties of narrow-gap semiconducting α-$SrSi_2$: A complementary experimental and first-principles hybrid-functional approach. J Appl Phys 129:115101. https://doi.org/10.1063/5.0041670

[26] Lue CS, Wong SF, Huang JY, Hsieh HL, Liao HY, Ramachandran B, Kuo YK (2013) Chemical pressure effect on thermoelectric properties of Ca and Ba substituted $SrSi_2$ alloys. J Appl Phys 113:013710. https://doi.org/10.1063/1.4772973

[27] Lue CS, Kuo CN, Huang JY, Hsieh HL, Liao HY, Ramachandran B, Kuo YK (2013) Enhancement of thermoelectric performance driven by Ge substitution in $SrSi_2$ alloy. J Phys D: Appl Phys 46:315303. https://doi.org/10.1088/0022-3727/46/31/315303

[28] Kuo YK, Lue CS, Hsu G, Huang JY, Hsieh HL (2012) Investigation of Al substitution on the thermoelectric properties of $SrSi_2$. Mater Chem Phys 137:604–607. https://doi.org/10.1016/j.matchemphys.2012.10.009

[29] Lue CS, Chou MD, Kaurav N, Chung YT, Kuo YK (2009) Enhancement in the thermoelectric performance by Y substitution on $SrSi_2$. Appl Phys Lett 94:192105. https://doi.org/10.1063/1.3136847

[30] Shiojiri D, Kunioka H, Iida T, Yamaguchi M, Hirayama N, Imai Y Factors limiting the thermoelectric performance of n- and p-type narrow band gap semiconducting α-$SrSi_2$. Available at SSRN: https://ssrn.com/abstract=4524635 or https://doi.org/10.2139/ssrn.4524635

[31] Giannozzi P, Baroni S, Bonini N, Calandra M, Car R, Cavazzoni C, Ceresoli D, Chiarotti GL, Cococcioni M, Dabo I, Corso AD, Gironcoli S, Fabris S, Fratesi G, Gebauer R, Gerstmann U, Gougoussis C, Kokalj A, Lazzeri M, Martin-Samos L, Marzari N, Mauri F, Mazzarello R, Paolini S, Pasquarello A, Paulatto L, Sbraccia C, Scandolo S, Sclauzero G, Seitsonen AP, Smogunov A, Umari P, Wentzcovitch RM QUANTUM ESPRESSO: a modular and open-source software project for quantum simulations of materials. J Phys Condens. Matter 21, 395502 (39). https://doi.org/10.1088/0953-8984/21/39/395502

[32] Perdew JP, Burke K, Ernzerhof M (1996) Generalized gradient approximation made simple. Phys Rev Lett 77:3865–3868. https://doi.org/10.1103/PhysRevLett.77.3865

[33] Evers J (1979) Phase diagram of SrSi$_2$ to 40 kbar and 1200 ∘C. J Phys Chem Solids 40:951–954. https://doi.org/10.1063/1.1849423

[34] Tokumaru Y, Okada Y (1984) Precise determination of lattice parameter and thermal expansion coefficient of silicon between 300 and 1500 K. J Appl Phys 56:314–320. https://doi.org/10.1063/1.333965

[35] Janzon K, Schafer H, Weiss A (1965) Crystal structure of strontium disilicide. Angew Chem, Int Ed Engl 4, 245. https://doi.org/10.1002/anie.196502452

[36] Imai M (2011) Thermal expansion of Alkaline-Earth-Metal disilicides AeSi$_2$ (Ae = Ca, Sr, and Ba). Jpn J Appl Phys 50:101801. https://doi.org/10.1143/JJAP.50.101801

[37] Cordero B, Gomez V, Platero-Prats AE, Reves M, Echeverria J, Cremades E, Barragan F, Alvarez S (2008) Covalent radii revisited. Dalton Trans 21:2832–2838. https://doi.org/10.1039/B801115J

[38] Palenzona A, Pani M (2004) The phase diagram of the Sr–Si system. J Alloy Compd 373:214–219. https://doi.org/10.1016/j.jallcom.2003.11.003

[39] Imai M, Abe E, Ye J, Nishida K, Kimura T, Honma K, Abe H, Kitazawa H (2001) Superconductivity of ternary silicide with the AlB$_2$-Type structure Sr(Ga$_{0.37}$,Si$_{0.63}$)$_2$. Phys Rev Lett. 87, 077003. https://doi.org/10.1103/PhysRevLett.87.077003

[40] Imai M, Nishida K, Kimura T, Abe H (2002) Superconductivity of ternary silicides A(Ga$_x$, Si$_{1-x}$)$_2$ (A = Ca, Sr, and Ba). Physica C 377:96–100. https://doi.org/10.1016/S0921-4534(01)01122-4

[41] Imai M, Nishida K, Kimura T, Kitazawa H, Abe H, Kitˆo H, Yoshii K (2002) Superconductivity of MI (MII$_{0.5}$,Si$_{0.5}$)$_2$ (MI = Sr and Ba, MII =Al and Ga), ternary silicides with the AlB$_2$-type structure. Physica C: Superconductivity 382, 361–366. https://doi.org/10.1016/S0921-4534(02)01798-7

[42] Meng RL, Lorenz B, Wang YS, Cmaidalka J, Sun YY, Xue YY, Meen JK, Chu CW (2002) Study of binary and pseudo-binary intermetallic compounds with AlB$_2$ structure. Physica C: Superconductivity 382, 113–116. https://doi.org/10.1016/S0921-4534(02)01208-X

[43] Shiojiri D, Iida T, Yamaguchi M, Hirayama N, Imai Y (2022) First-principles study of the effects of native defects on the thermoelectric properties of narrow- gap semiconducting α-SrSi$_2$ using the hybrid functional method. Physica B 634:413795. https://doi.org/10.1016/j.physb.2022.413795